RESEARCH ARTICLE

Dynamic 2D and 3D mapping of hyperpolarized pyruvate to lactate conversion in vivo with efficient multi-echo balanced steady-state free precession at 3 T

Christoph A. Müller[1,2] | Christian Hundshammer[3,4,5] | Miriam Braeuer[3] |
Jason G. Skinner[1,3] | Stephan Berner[1,2] | Jochen Leupold[1] | Stephan Düwel[3] |
Stephan G. Nekolla[3] | Sven Månsson[6] | Adam E. Hansen[7] |
Dominik von Elverfeldt[1] | Jan H. Ardenkjaer-Larsen[8] | Franz Schilling[3] |
Markus Schwaiger[3] | Jürgen Hennig[1] | Jan-Bernd Hövener[1,9]

[1]Department of Radiology, Medical Physics, Medical Center - University of Freiburg, Faculty of Medicine, University of Freiburg, Freiburg, Germany

[2]German Consortium for Translational Cancer Research (DKTK), Partnersite Freiburg, German Center for Cancer Research (DKFZ), Heidelberg, Germany

[3]Department of Nuclear Medicine, University Hospital rechts der Isar, Munich, Germany

[4]Department of Chemistry, Technical University of Munich, Garching, Germany

[5]Munich School of Bioengineering, Technical University of Munich, Garching, Germany

[6]Medical Radiation Physics, Department of Translational Medicine, Lund University, Skåne University Hospital, Malmö, Sweden

[7]Department of Clinical Physiology, Nuclear Medicine & PET, Rigshospitalet, University of Copenhagen, Denmark

[8]Department of Electrical Engineering, Technical University of Denmark, Kgs Lyngby, Denmark

[9]Section Biomedical Imaging, Molecular Imaging North Competence Center (MOIN CC), Department of Radiology and Neuroradiology, University Medical Center

Abstract

The aim of this study was to acquire the transient MRI signal of hyperpolarized tracers and their metabolites efficiently, for which specialized imaging sequences are required. In this work, a multi-echo balanced steady-state free precession (me-bSSFP) sequence with Iterative Decomposition with Echo Asymmetry and Least squares estimation (IDEAL) reconstruction was implemented on a clinical 3 T positron-emission tomography/MRI system for fast 2D and 3D metabolic imaging. Simulations were conducted to obtain signal-efficient sequence protocols for the metabolic imaging of hyperpolarized biomolecules. The sequence was applied in vitro and in vivo for probing the enzymatic exchange of hyperpolarized $[1-^{13}C]$pyruvate and $[1-^{13}C]$lactate. Chemical shift resolution was achieved using a least-square, iterative chemical species separation algorithm in the reconstruction. In vitro, metabolic conversion rate measurements from me-bSSFP were compared with NMR spectroscopy and free induction decay-chemical shift imaging (FID-CSI). In vivo, a rat MAT-B-III tumor model was imaged with me-bSSFP and FID-CSI. 2D metabolite maps of $[1-^{13}C]$pyruvate and $[1-^{13}C]$lactate acquired with me-bSSFP showed the same spatial distributions as FID-CSI. The pyruvate-lactate conversion kinetics measured with me-bSSFP and NMR corresponded well. Dynamic 2D metabolite mapping with me-bSSFP enabled the acquisition of up to 420 time frames (scan time: 180-350 ms/frame) before the hyperpolarized $[1-^{13}C]$pyruvate was relaxed below noise level. 3D

Schleswig Holstein (UKSH), Kiel University, Germany

Correspondence
Christoph A. Müller and Jan-Bernd Hövener, Department of Radiology, Medical Physics, Medical Center - University of Freiburg, Faculty of Medicine, University of Freiburg, Freiburg. Germany.
Email: christoph.mueller.rdiag@uniklinik-freiburg.de; Jan.Hoevener@rad.uni-kiel.de

metabolite mapping with a large field of view ($180 \times 180 \times 48$ mm^3) and high spatial resolution ($5.6 \times 5.6 \times 2$ mm^3) was conducted with me-bSSFP in a scan time of 8.2 seconds. It was concluded that Me-bSSFP improves the spatial and temporal resolution for metabolic imaging of hyperpolarized [$1-^{13}$C]pyruvate and [$1-^{13}$C]lactate compared with either of the FID-CSI or EPSI methods reported at 3 T, providing new possibilities for clinical and preclinical applications.

KEYWORDS
carbon-13, balanced steady-state free precession, dynamic nuclear polarization, hyperpolarization, metabolite mapping, magnetic resonance imaging

1 | INTRODUCTION

Nuclear magnetic resonance (NMR) is a versatile phenomenon that is used for chemical analysis and in vivo imaging alike. However, the chemical or spectroscopic information of the magnetic resonance (MR) signal is only rarely used for clinical routine diagnostics.[1]

The reason for this is that usually the MR signal of metabolites has a very low signal-to-noise ratio (SNR). Thus, the chemical, spatial and temporal resolutions in MR spectroscopic imaging (MRSI) are typically limited to mM concentrations, cubic centimeters and minutes in clinical settings in vivo.[1]

MR signal enhancement by hyperpolarization can temporarily help to overcome these limits by providing transient signal enhancements of several orders of magnitude. Hyperpolarization of biomolecules with dissolution dynamic nuclear polarization (dDNP)[2] has provided a direct window into the metabolism of living organisms.

To take full advantage of the benefits promised by hyperpolarization, specialized acquisition methods are required: the hyperpolarized (HP) magnetization is short-lived and inevitably decays back to the low, thermal equilibrium within minutes at most. While a high spatial, temporal and spectral resolution is desired in the MR images, the HP magnetization available is limited and must be handled with care. In addition, dynamic measurements with high temporal resolution are desired for observation of the metabolic conversion. This requires reduced usage of the HP magnetization per scan as well. The goal is to maintain a long acquisition window in which the biomolecules are visible.

Accordingly, several sequences have been suggested to acquire spectral and spatial information at the same time with a different emphasis on one or the other. Nonlocalized methods provide high spectral information of a given volume defined by the sensitive volume of the coil without further spatial discrimination.[3] Single-voxel methods use spatial selective excitation of one defined volume element (voxel) acquired at high spectral resolution.[4] In chemical shift imaging (CSI),[5-7] most of the data are typically acquired in the spectral dimension (10^3 data points), while the spatial domain is small and in the order of 10^2 voxels (eg, an 8×8 or 16×16 matrix). The temporal resolution is limited and is given by the number of image voxels. In comparison, echo planar spectroscopic imaging (EPSI) sequences[8,9] provide improved temporal resolution, while the spatial resolution is similar and the spectral width is reduced (10^1-10^2 samples). EPSI is often used in clinical applications.[10-13]

At the other extreme, there are sequences that acquire full spatial but minimal spectral resolution. These methods include Dixon techniques, where only a few spectral points are acquired, for example, to produce one image of fat and one image of water.[14-17] Multi-point Dixon techniques use an iterative reconstruction method that allows the reconstruction of images at specific predefined chemical shifts.[18,19] Instead of acquiring full free induction decays (FIDs), this allows acquisition of fast spiral CSIs with few spectral points if prior knowledge about the resonance frequencies exists.[20-23] Several improvements have been suggested, including reducing the effect of T_2^*-relaxation,[24] multiple lipid resonances[25] and phase errors induced by bipolar gradients.[26]

Iterative Decomposition with Echo Asymmetry and Least squares estimation (IDEAL) was previously used to accelerate CSI[20-22] and to reconstruct multi-echo balanced steady-state free precision (bSSFP) data. The bSSFP is one of the most efficient imaging sequences in terms of SNR and magnetization usage. Fast ^{1}H frequency mapping for thermometry,[27] chemical shift maps of thermally polarized ^{1}H and ^{31}P and HP ^{13}C were successfully acquired with me-bSSFP at 1.5 T,[28,29] and 3D spatial-spectral MR imaging with me-bSSFP at 1.5 T was conducted in a rat in vivo with a HP but metabolically inert ^{13}C reagent.[30] Single-frequency bSSFP (without multi-echoes) was used for consecutively imaging individual HP

metabolites in vitro and in vivo.[31-33] After the initial publications,[28,29] the advantages promised by me-bSSFP and IDEAL reconstruction were never fully analyzed or explored. In this work, we investigate me-bSSFP-IDEAL at 3 T. We applied the technique in a hyperpolarization-PET-MRI study to image the Warburg effect by observing the exchange of $[1-^{13}C]$pyruvate and $[1-^{13}C]$lactate (denoted as pyruvate and lactate). Compared with previous results, the spatial and temporal resolution were substantially improved, such that observation of the metabolic conversion in one slice or 3D metabolite mapping became possible.

2 | METHODS

2.1 | Pulse sequences

A bSSFP (TrueFISP, FIESTA)[34] sequence with alternating $\pm\alpha$ pulses and a multi-echo (me) readout was implemented as previously described.[29] Instead of dummy cycles, an $\alpha/2$ excitation pulse was applied TR/2 before the first α pulse to reduce transient signal oscillations.[35] TR/2 after the last α pulse of the sequence, an $\alpha/2$ tip-back pulse was applied to tip the magnetization parallel to B_0. Gaussian-shaped pulses with a length of 1-2 ms with transmitter frequency centered between pyruvate and lactate were used, such that both resonances were excited equally.

Between the pulses, a balanced bipolar multi-gradient echo (me) readout was implemented (Figure 1). During each me-readout, N_E echoes were acquired, separated by the time ΔTE, yielding a spectral width of $SW = 1/\Delta TE$ and a spectral resolution of $\Delta SW = SW/N_E$. Between pulse and me-readout, gradients encode N_P phase steps to navigate through k-space in centric line ordering. For 2D MRI, N_S slices were acquired by applying gradients during excitation. 3D encoding was achieved with global excitation and additional N_S phase-encoding gradients in the slice direction. The total acquisition time per time frame TA amounted to $N_P \times N_S \times TR + 2 \times TR/2$.

2.2 | Simulation of bSSFP

To investigate and predict the behavior of the bSSFP signal and to identify suitable sequence parameters, the signal was simulated with Bloch equations in Matlab (Mathworks, Natick, MA) using the formalism previously described.[36] A bSSFP pulse train, $(\alpha/2) - (\mp\alpha \times 32) - (-\alpha) - (\alpha/2)$, was simulated for variations of flip angles from $\alpha = 1°-180°$ and repetition times from TR = 5-30 ms. The evolution of 1024 individual spins (isochromats) was simulated and recorded at the echo time TE = TR/2 for each repetition. The precession frequencies of different isochromats were Lorentzian-distributed around a center ω with a peak-width $\Delta\omega$. For each echo, the magnetization vectors of the isochromats were summed to yield the total 3D magnetization M_{xyz}. Relaxation constants were measured by NMR or estimated (Table S1, Figures S1 and S2). The starting magnetization M_s was set to either the thermal equilibrium, $M_{eq} = M_s = 0, 0, 1$, or to a HP state that was 30 000-fold enhanced $M_s = 0, 0, 30 \times 10^3$, corresponding to a hyperpolarization of ~ 8% at 3 T and room temperature, respectively.

2.3 | MR systems

Experimental validation of simulations of thermally polarized samples was performed on a whole-body 3 T MR system (MAGNETOM Trio, Siemens) equipped with a transmit-and-receive ^{1}H-^{13}C volume coil (Rabbit Volume Coil, Rapid Biomedical) in quadrature design with 170 mm inner diameter (Ø), 305 mm length and ^{13}C transmit reference amplitude for a 1 ms 90° block pulse of 105 V.
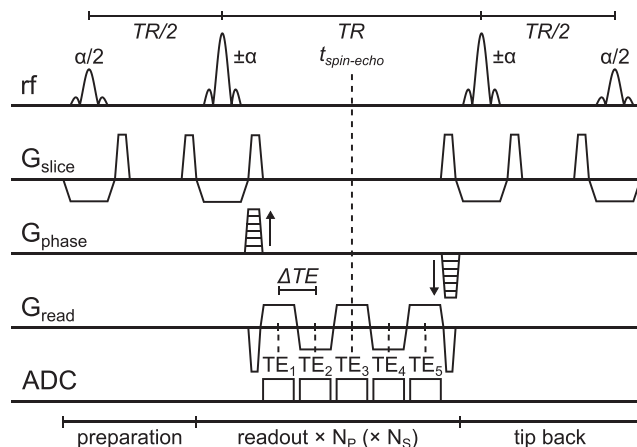
FIGURE 1 Schematic view of a 2D me-bSSFP sequence with an $\alpha/2$ pulse for preparation, α pulses with alternating phase to create spin echoes at the time $t_{spin-echo}$, and an α-$\alpha/2$ "tip-back" module after acquisition for conservation of magnetization. All gradient zeroth moments are balanced out between successive pulses. The sequence is repeated until all phase steps are sampled. A bipolar multi-echo readout in read-dimension samples the same k-space line at NE time points $[TE_1 - TE_{Ne}]$, to gather the information for later chemical shift separation

FIGURE 2 Summed simulated signal intensity of thermally polarized urea (A) and lactate (B) for bSSFP as a function of TR and flip angle. Periodically repeating signal voids were observed as a function of TR (dashed lines, eg, TR = 10, 16, 24 ms), similarly for both metabolites. Experiments were conducted for fixed flip angle or TR (A1, B1-3), and the simulated results were well reproduced

In vitro and in vivo ^{13}C MRSI was performed on a 3 T whole-body MR-PET system (mMR Biograph, Siemens) with a gradient system capable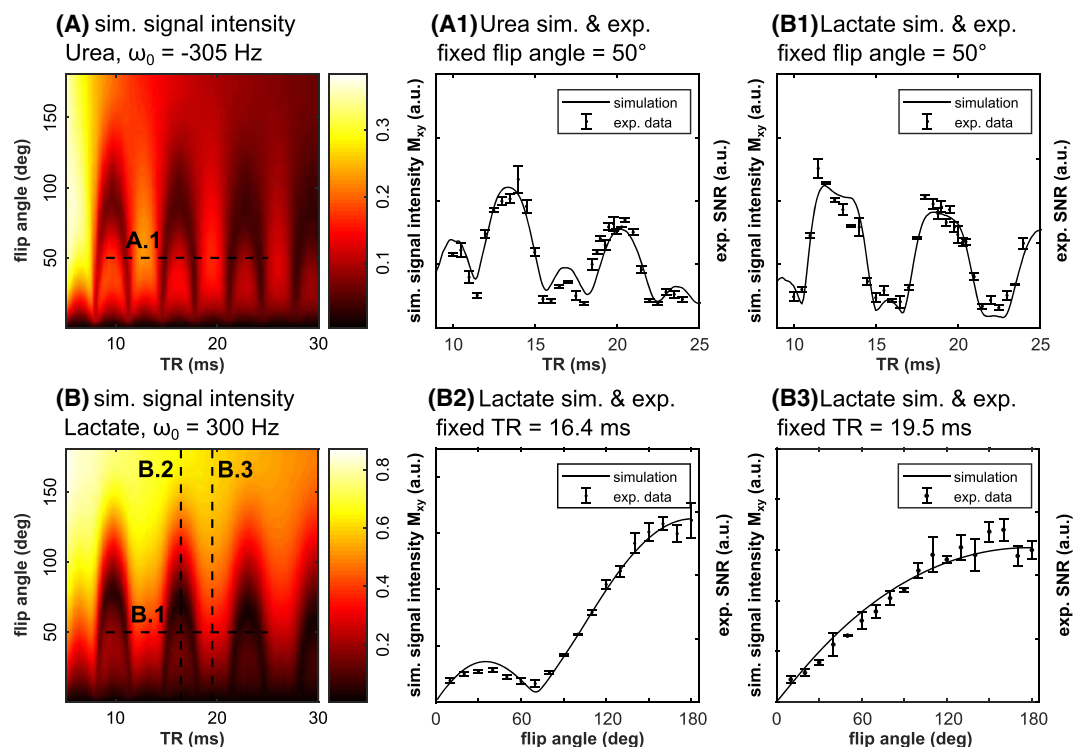 of max. 40 mT/m at 180 mT/m/s, equipped with a transmit-and-receive ^{1}H-^{13}C surface coil: size ^{1}H rectangle = 180 × 244 mm, ^{13}C loop = 110 mm Ø (dual-tuned flexible surface coil, Rapid Biomedical). The ^{13}C transmit amplitude of the surface coil for a 1 ms 90° block pulse was calibrated to 30 V.

Shimming up to second order was applied at the beginning of each MRI or MRSI session. The transmit-and-receive frequencies and transmit reference amplitude were adjusted manually for each coil after shimming using a thermally polarized model solution (MS) containing lactate (MS1) or urea (MS2).

A 1 T Spinsolve Carbon benchtop NMR (Magritek, Aachen, Germany) was used for spectroscopy with 5 mm tubes.

2.4 | Model solutions

For experiments in thermal equilibrium, two MSs of 5 mL volume were prepared in cylindrical glass vials containing either 2.23 M [1–^{13}C] lactate (MS1) or 4 M [^{13}C]urea (denoted as urea) (MS2), supplemented with 0.23% (v/v) gadoteric acid (Dotarem, Gueberet Laboratories) and 0.15% (w/v) NaN$_3$, both at physiological pH of ~ 7. MS1 was placed in the FOV in vitro and in vivo to adjust the scanner frequency before the injection and for quality assurance of the reconstruction. Chemicals were purchased and used without further purification unless stated otherwise (Cambridge Isotope Laboratories, Tewksbury, MA; Sigma Aldrich, St. Louis, MO). Lactate dehydrogenase (LDH) and nicotinamide adenine dinucleotide (NAD$^+$ or NADH) were purchased from Sigma Aldrich.

2.5 | Hyperpolarization of pyruvate

[1–^{13}C]pyruvate (denoted as pyruvate) was supplemented with 15 mM OX063 trityl radical (Oxford Instruments), 1 mM gadoteric acid (Dotarem) and HP by dDNP (HyperSense, Oxford Instruments). Microwaves with a frequency of 94.172 GHz and 100 mW were used for irradiation. After ~ 30 minutes at 1.2 K, the sample was dissolved in a buffered solution pressurized to 100 kPa and heated to 180°C. Final concentrations, dissolution buffer compositions, and the pH of the final dissolution solution containing pyruvate, are given in Table S3.

The final solution was injected either into vials or tubes for in vitro experiments (Table 1), or into an animal via a catheter for in vivo imaging.

2.6 | Cell culture and animal handling

Subcutaneous tumors were induced at the right flank of Fischer 344 rats (Charles River) aged 6 weeks with an average weight of ~ 130 g by implantation of 1×10^6 13762 MAT B III breast cancer cells derived from mammary adenocarcinoma. For this purpose, cells were cultivated in RPMI-1640 medium supplied with 10% fetal calf serum, 1% penicillin and 1% streptomycin and resuspended in 200 μL McCoy's 5A medium for implantation.

The animals underwent imaging 13 days after tumor implantation. Anesthesia was performed with 1%-3% isoflurane, a tail-vein catheter was placed, and the animal was positioned in the isocenter of the PET-MR. Blood oxygenation (Expression MR Patient Monitor, Invivo, Gainesville, FL) and breathing rate (ECG Trigger Unit, Rapid Biomedical, Rimpar, Germany) were continuously monitored during the experiments. The temperature of the animal was maintained using a warming blanket set to 38°C (Mistral-Air Neonatal Plus, The 37Company, Amersfoort, the Netherlands). All animal experiments were approved by the local governmental committee for animal protection and welfare (Tierschutzbehörde, Regierung Oberbayern).

2.7 | ^{13}C imaging experiments

The following protocols were used for ^{13}C MRSI. All sequence parameters can be directly compared in Table S2 (see the supporting information).

2.7.1 | Protocol 1: simulations and experimental verification

Simulations were compared with bSSFP imaging of thermally polarized MSs on the 3 T MR system: TR = 16.4 or 19.5 ms, FOV = 180 × 180 x 50 mm^3, base resolution = 32 × 32 × 1, image matrix = 64 × 64 × 1, image resolution = 2.8 × 2.8 × 50 mm^3, one echo, TE = TR/2, TA ~ 0.54 or 0.64 seconds. The flip angle was varied for different experiments between α = 10°-180° and each scan was repeated three times, interleaved by a pause of 60 seconds to reinstate thermal equilibrium. The slice thickness of 5 cm was chosen to include and excite the entire MS. SNR was measured and manually scaled by an overall constant factor to match the simulations.

2.7.2 | Protocol 2: measurement of the decay of hyperpolarization during ^{13}C imaging

Pyruvate was HP, transferred to the 3 T PET-MR system, injected into prepared vials, and measured with FID-CSI or me-bSSFP. Experimental protocol for FID-CSI: α = 10°, TR = 180 ms, FOV = 80 × 80 × 13 mm^3, base resolution = 8 × 8 × 1 with elliptical k-space sampling (ie, 29 excitations), image matrix = 32 × 32 × 1, image resolution = 2.5 × 2.5 × 13 mm^3, spectral points = 512, spectral width = 3000 Hz, TA = 5.1 seconds. Experimental protocol for me-bSSFP: α = 20°, TR = 10.64 ms, FOV = 160 × 160 × 10 mm^3, base resolution = 16 × 16 × 1, image matrix = 32 × 32 × 1, image resolution = 5 × 5 × 10 mm^3, five echoes, TE_1 = 2.96 ms, ΔTE = 1.18 ms, TA = 0.18 seconds (Table S2, P 2). The sequences were applied continuously for 5 seconds (28 time frames of me-bSSFP or one CSI scan) followed by a 5-second pause. Per me-bSSFP scan, one α/2 excitation, 16 ± α refocusing and one −α−α/2 tip-back pulse were played out. For CSI, 29 excitations were used to acquire one image. Note that the number of excitations per 5-second block is nearly the same for CSI and me-bSSFP (disregarding the refocusing pulses of me-bSSFP). Prior to the injection of HP pyruvate, the vial was filled with aqueous solution and placed on top of the surface coil. All adjustments were performed prior to the injections. The sequences were started after the injection was finished, and the slices were oriented perpendicular to the vial. For reproducibility, all scans were repeated three times with freshly HP pyruvate. Finally, a mono-exponential decay function was fitted to the HP signal intensities to extract the apparent decay rate constant of the HP signal.

TABLE 1 Pipette scheme for hyperpolarized in vitro measurements

	In vitro hyperpolarization decay measurement	In vitro LDH activity measurement (FID-CSI, me-bSSFP, NMR*[*])
V (pyruvate)/μL	2000	500
V (buffer)/μL	5000	4800
V (250 mM NADH)/μL	-	320
c (LDH)/μg*mL^{-1}	-	4.00, 8.00, 11.98, 15.96

Abbreviations: c, concentration; FID-CSI, free induction decay-chemical shift imaging; LDH, lactate dehydrogenase; me-bSSFP, multi-echo balanced steady-state free precession; NADH, reduced nicotinamide adenine dinucleotide; NMR, nuclear magnetic resonance; V, volume.
[*]The in vitro LDH activity measurements at the NMR system were conducted with 10-fold reduced volumes but the same concentrations.

2.7.3 | Protocol 3: NMR of pyruvate-lactate exchange in vitro (NMR and PET-MR)

For NMR experiments, pyruvate was HP and injected into a 5 mm tube filled with LDH solution inside the NMR spectrometer (concentrations in Table 1). A pulse-acquire sequence was started after the injection (FID: α = 5°, TR = 2000 ms, spectral points = 1024, spectral width = 5000 Hz, TA = 2 seconds, 200 consecutive acquisitions). The experiment was repeated three times for each concentration from Table 1.

For MRSI experiments, 23 ± 2 seconds after dissolution, one batch of HP pyruvate was injected into four vials one at a time placed inside the isocenter of the PET-MR. Each vial was prepared beforehand with different amounts of LDH and NADH (Table 1). Then, 15 ± 2 seconds before the first injection, FID-CSI or bSSFP imaging commenced (CSI: α = 15°, TR = 200 ms, FOV = 80 × 80 × 13 mm^3, base resolution = 8 × 8 × 1 with elliptical k-space sampling, image matrix = 32 × 32 × 1, image resolution = 2.5 × 2.5 × 13 mm^3, spectral points = 512, spectral width = 3000 Hz, TA = 5.8 seconds, 40 consecutive scans acquired every Δt = 6 seconds; me-bSSFP: α = 60°, TR = 10.64 ms, FOV = 180 × 180 × 10 mm^3, base resolution = 32 × 32 × 1, image matrix = 64 × 64 × 1, image resolution = 2.8 × 2.8 × 10 mm^3, five echoes, TE$_1$ = 2.96 ms, ΔTE = 1.18 ms, TA = 0.35 seconds). For a total of 256 seconds, one scan was started every second (256 images). The experiment was repeated three times with freshly prepared LDH and NADH solutions and HP pyruvate.

2.7.4 | Protocol 4: 2D in vivo imaging (PET-MR)

In vivo, 1.0 ± 0.1 mL of ~ 90 mM HP pyruvate was injected ~ 24 ± 7 seconds after dissolution into a tail vein catheter of an anesthetized rat carrying a subcutaneous tumor, lying on the surface coil inside the 3 T PET-MR (head first, right lateral). At the onset of the injection, FID-CSI or me-bSSFP was started with the parameters of protocol 3 (see section 2.7.3). FID-CSI or me-bSSFP sequences were acquired every 6 or 2 seconds, respectively, for a total of 120 seconds each. MS1 was placed next to the animal and all scanner settings were adjusted beforehand.

2.7.5 | Protocol 5: in vivo 3D pyruvate-lactate mapping (PET-MR)

Approximately 19 seconds after dissolution, 1.0 ± 0.1 mL of ~ 90 mM HP pyruvate was injected into the tail vein of the animals carrying a subcutaneous tumor placed on the surface coil (head first, right lateral). 3D me-bSSFP was started with the injection, and three 3D datasets were acquired in a row without pause (α = 80°, TR = 10.64 ms, FOV = 180 × 180 × 48 mm^3, base resolution = 32 × 32 × 24, image matrix = 64 × 64 × 24, image resolution = 2.8 × 2.8 × 2 mm^3, five echoes, TE$_1$ = 2.96 ms, ΔTE = 1.18 ms, TA = 8.2 seconds). The scanner was adjusted beforehand using the signal of the animal and MS1.

2.8 | Data postprocessing and analysis

2.8.1 | Reconstruction and quantification of me-bSSFP metabolite maps

The separation of the chemical species from multi-point sequences, as described by Reeder et al,[18] Yu et al[24] and Peterson and Månsson[26] was implemented in a graphical user interface (Matlab, Mathworks). For the IDEAL reconstruction with estimation of a B$_0$ field map and a bipolar echo-correction map, five echoes was the minimum number to reconstruct three metabolite maps, namely, pyruvate, pyruvate hydrate and lactate.[26] The time difference between echoes in me-bSSFP was chosen to be as short as possible, but such that the effective number of signal averages was 4.4 for the chemical shifts of pyruvate and lactate, and also that the gradient amplitudes and switching were still realizable.[18]

Prior to IDEAL, complex valued images for each echo time were reconstructed in Matlab from raw k-space data. Two-fold in-plane zero filling was applied and the k-space edges were suppressed by multiplying the original k-space with a central lobe of a 2D sinc-function. The k-spaces of all even echoes were manually shifted by one voxel in the read direction to align the k-space centers of the odd and even echoes. This was needed to correct the asymmetric sampling with 16 or 32 points per readout.

During IDEAL, all complex echo images were used to separate lactate and pyruvate signals in each voxel at the relative frequencies of ±186 Hz (± 6 ppm at 3 T). A pyruvate hydrate map was reconstructed at the frequency +76 Hz, but was not analyzed further. IDEAL was iterated 10 times and the final estimations of the B$_0$ field and phase error maps were subsequently used for generating the metabolite maps.

Signal was quantified using the mean magnitude signal of all voxels in the region of interest (ROI). SNR was quantified by dividing the signal of an ROI by the standard deviation of noise in an apparently signal-free area in the same image (Matlab).

2.8.2 | Reconstruction and quantification of CSI maps

The elliptical k-space data were smoothed at the edges and interpolated to a square 16 × 16 k-space by the manufacturer's image reconstruction software (Siemens). A 2-fold zero filling was applied in the FID domain prior to fast Fourier transformation (FFT) in Matlab.

The signals of pyruvate and lactate were quantified by numerical integration over a range of ±50 Hz around the relative precession frequencies of ±186 Hz (± 6 ppm at 3 T) in each voxel to generate metabolite maps. For coregistration with anatomical in vivo images, these maps were resized with bicubic interpolation to 32 × 32 voxels.

2.8.3 | Reconstruction and quantification of NMR spectra

The NMR spectra and the pyruvate and lactate intensities in each spectrum—extracted from the peak height—were calculated using the software Mestre Nova (Mestrelab Research, Santiago de Compostela, Spain).

2.8.4 | Conversion rate constant quantification

For our specific study, to estimate LDH rate constants from the dynamic measurements in vitro and in vivo, the obtained pyruvate and lactate signals were plotted against time and integrated to obtain the areas under each curve (AUC). The AUCs were used to calculate the lactate-to-pyruvate ratio (LP ratio).[37-53]

2.8.5 | Measurement of the decay of hyperpolarization

A mono-exponential decay function was fitted to the obtained signals to extract the apparent decay rate constant of the hyperpolarization. The effect of excitation pulses was not taken into account, because CSI and bSSFP were set to employ the same number of excitation pulses.

3 | RESULTS

3.1 | Analyzing the bSSFP signal response

To investigate the effects of off-resonances in HP imaging, we simulated the bSSFP signal as a function of TR and flip angle for different metabolites with different frequencies and relaxation constants (Figure 2A,B). As expected, the strongest signal was observed for 180° pulses and short TRs, and periodically repeating signal minima were observed as a function of TR. The (simulated) signals of thermally polarized urea and lactate were found to respond similarly, but with different intensities.

These results were validated experimentally for a fixed flip angle or fixed TR (Figure 2A1,2B1-3). A high correlation between experiments and simulations was found, with Pearson pairwise linear correlation coefficients (ρ) of 0.94, 0.98, 1.00 and 0.98 and *P*-values of 1.5 x 10^{-15}, 1.7 x 10^{-13}, 1.3 x 10^{-17} and 3.5 x 10^{-13} for the data in Figure 2A1,B1-3, respectively (Figure S3). These results indicate that the simulations are accurately describing the bSSFP signal.

In the next step, the simulations were used to identify parameters for imaging HP pyruvate and lactate. Again, an alternating signal pattern was observed, with periodically repeating minima over TR (Figure 3).

For two settings of TR, 10.64 and 16.12 ms, we investigated the signal evolution of HP signal within one sequence (Figure 3A1,A2): for TR = 10.64 ms, a smooth signal evolution was observed throughout the sequence for all flip angles. For TR = 16.12 ms, signal variations were observed at the beginning of the pulse train, and signal cancelation occurred between flip angles of 50° and 100°. Thus, we chose TR = 10.64 ms for later experiments, providing higher and more stable signal over different flip angles.

3.2 | Decay of hyperpolarization during ^{13}C imaging

To investigate for how long the HP signal can be observed, pyruvate was HP and measured dynamically with FID-CSI or me-bSSFP for 150 seconds at 3 T (PET-MR, protocol 2). During this time, 15 FID-CSI images or 420 me-bSSFP images were acquired. The signal was quantified and a
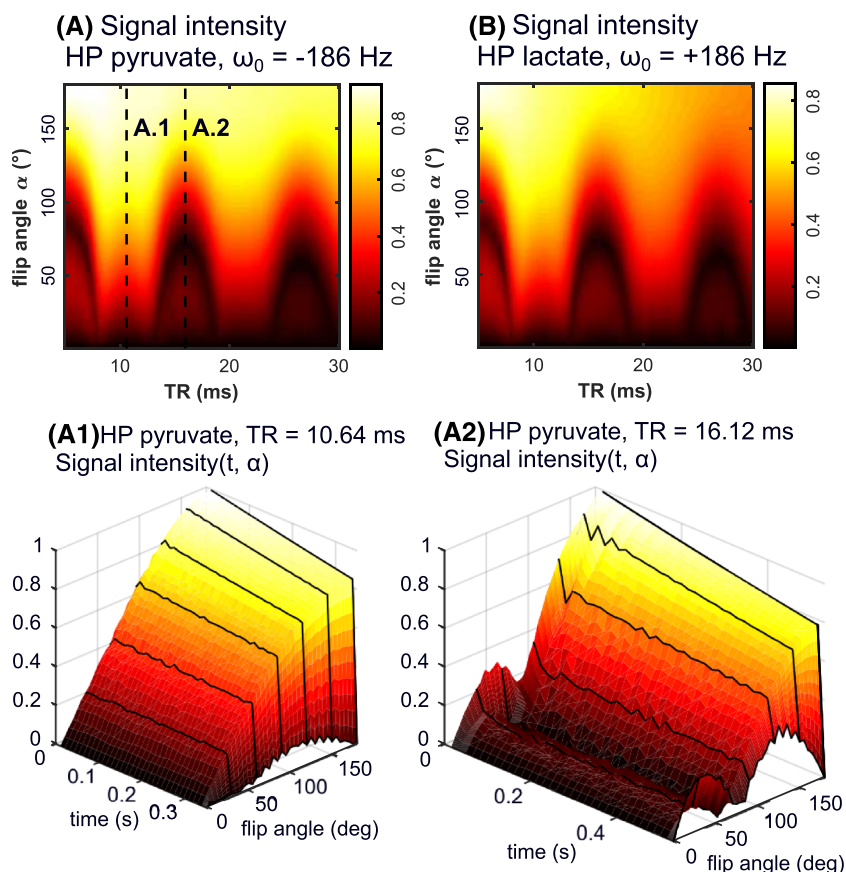
FIGURE 3 Simulated normalized me-bSSFP signal intensity for hyperpolarized pyruvate (A) and lactate (B) as a function of TR and flip angle. Periodically repeating signal voids were observed, and both metabolites exhibited a similar response. A and B show the sum of signal over a full sequence. For TR = 10.64 ms (A1) and 16.12 ms (A2), the pyruvate signal evolution over one me-bSSFP scan time was investigated. Note the decreased signal at flip angles around 90° for me-bSSFP with TR = 16.12 ms, which is not the case for me-bSSFP with TR = 10.64 ms. The lactate signal evolution over a scan time is analogous

mono-exponential function was fitted to the data, resulting in decay constants (τ) of 32.5 ± 0.7 and 34.5 ± 0.3 seconds for FID-CSI and me-bSSFP, respectively (Figure 4). Without tip-back pulses in the me-bSSFP sequence, τ = 26.6 ± 0.2 seconds was found.

3.3 | In vitro pyruvate-lactate exchange

The enzymatic conversion of HP pyruvate to lactate was measured dynamically in vitro with NMR, FID-CSI and me-bSSFP in solutions containing 4, 8, 12 and 16 µg/mL lactate dehydrogenase in water (PET-MR and NMR, protocol 3).

For NMR, the solutions were measured one at a time, each for a total of 400 seconds. Every other second, one 5° spectrum was acquired. For FID-CSI, 40 images were acquired in a total of 240 seconds, one every 6 seconds (TA = 5.1 seconds). For me-bSSFP, one image was acquired every second for 256 seconds (TA = 0.35 seconds). A selection of the metabolite maps from me-bSSFP and FID-CSI are shown in Figure 5. Movie S1 shows a time lapse through all frames from one me-bSSFP acquisition together with the signal intensities of pyruvate and lactate in each of the vials.

All methods showed the expected pyruvate-lactate exchange and decaying HP. The imaging methods provided maps of pyruvate and lactate, and HP signal (lactate) was observed for ~ 190 seconds and more than 240 seconds for FID-CSI and me-bSSFP, respectively. Because of the large differences in signal strength during the decay, each image was scaled to its maximum. As a result, the signal of the thermally polarized MS1 solution (vial 5) appears to increase with time.

The pyruvate and lactate signals were quantified and exhibited the expected curves for NMR and me-bSSFP, where a pyruvate maximum is followed by a lactate maximum (Figure 6). The FID-CSI signal does not show this feature. Instead, the maxima of pyruvate and lactate coincide.

The area under the curves were measured, and an affine-linear function $f(c) = mc+b$ was fitted to the LP ratios as function of LDH concentration c, yielding slopes of m = 0.05 ± 0.06 µg/mL (b = −0.13 ± 0.73, R^2 = 0.883), 0.014 ± 0.004 µg/mL (b = 0.19 ± 0.04, R^2 = 0.991) and 0.035 ± 0.004 µg/mL (b = −0.01 ± 0.06, R^2 = 0.995) for me-bSSFP, FID-CSI and NMR, respectively.

The NMR data yielded the most robust fit and an offset (b) close to 0, as expected. Me-bSSFP yielded a similar slope, but with a larger variance. The variance was low for FID-CSI, but the conversion rate was strongly underestimated, in addition to a large nonzero offset. This may be caused by the coarse spatial resolution and broad spatial point spread function.

FIGURE 4 ^{13}C MRSI signal of hyperpolarized pyruvate acquired dynamically with FID-CSI (A, 15 images) and me-bSSFP (B, 420 images). A mono-exponential decay function was fitted to the data and yielded apparent decay constants, τ = 33 and 35 seconds, for FID-CSI and me-bSSFP, respectively (dashed lines). While both methods provided a similar temporal observation window, 28-fold more images were produced by me-bSSFP. Each indicator represents the mean of three experiments. Error bars indicate the standard deviation
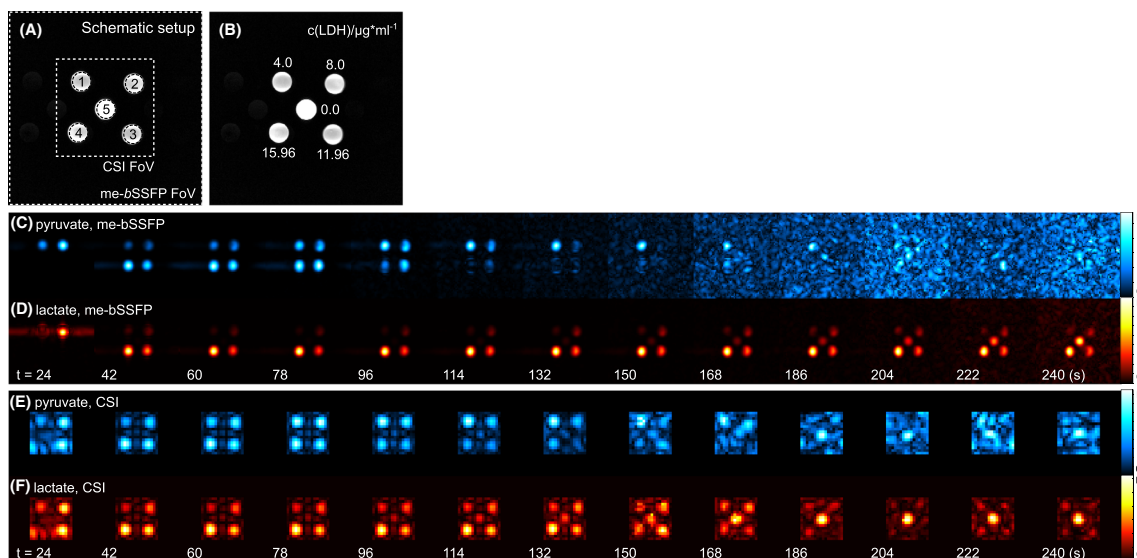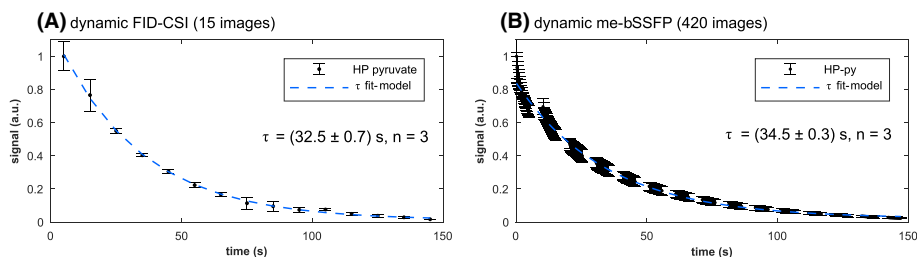

(A) dynamic FID-CSI (15 images)

HP pyruvate
τ fit-model

τ = (32.5 ± 0.7) s, n = 3

(B) dynamic me-bSSFP (420 images)

HP-py
τ fit-model

τ = (34.5 ± 0.3) s, n = 3

FIGURE 5 ^{1}H-MRI (A, B) and ^{13}C-MRSI (C-F) of hyperpolarized pyruvate (blue) and lactate (red) exchange in vitro. Four vials with different amounts of LDH (1–4) and lactate model solution MS1 (5) were placed in the 3 T PET-MR (A, B). Pyruvate was hyperpolarized, injected into the vials and measured with me-bSSFP (C, D) or FID-CSI (E, F). The acquisitions started ~ 10 seconds before the injection. One me-bSSFP image was acquired every second, and one FID-CSI every 6 seconds. Note that each image was individually scaled to its maximum (M) and that the FOVs were different. At 24 seconds, the second vial (in C, D) and the third vial (in E, F) were just filled with HP pyruvate by the ongoing injection process. For me-bSSFP, a disturbance of the B_0-field by the pipette likely caused the smearing artefact of vial 2 in the phase direction (left to right). The diameter of each vial was ~ 1.5 cm

3.4 | In vivo pyruvate-lactate exchange

HP pyruvate was injected ~ 24 seconds after dissolution into tumor-bearing animals and metabolite maps were acquired with me-bSSFP or FID-CSI at 3 T (PET-MRI, protocol 3). Both sequences detected HP pyruvate and lactate signal in the animal (Figure 7). A movie that shows all frames of the me-bSSFP acquisition is provided online (Movie S2). The higher spatial resolution of me-bSSFP allowed better differentiation between abdominal aorta and tumor than the FID-CSI images, whose voxels were ~ 4-fold larger. The strongest pyruvate signal was found at the abdominal aorta, while the most lactate signal was found in the cancerous tissue. The SNR of pyruvate in the tumor, lactate in the tumor and lactate in the vial was quantified to 85.2, 12.6 and 11.2 for me-bSSFP, and 11.04, 10.93 and 7.49 in the FID-CSI maps, respectively, at peak pyruvate signal (22 and 29 seconds after start of injection for me-bSSFP and FID-CSI, respectively). At its maximum, the signal of HP lactate reached a similar intensity to the thermally polarized 2.23 M lactate (MS1) next to the animal. Both methods accurately depicted the lactate MS, indicating a reliable metabolite separation.

The quantified signals exhibited a distinct pyruvate maximum followed by a broader lactate maximum (Figure 7B,C). The areas under the curves were quantified and yielded an LP ratio of 0.34 and 0.17 for me-bSSFP and FID-CSI, respectively. Fitting a mono-exponential decay function to the pyruvate signal in the tumor after peak yielded similar decay rate constants of 14.4 ± 0.5 and 13.9 ± 1.5 seconds
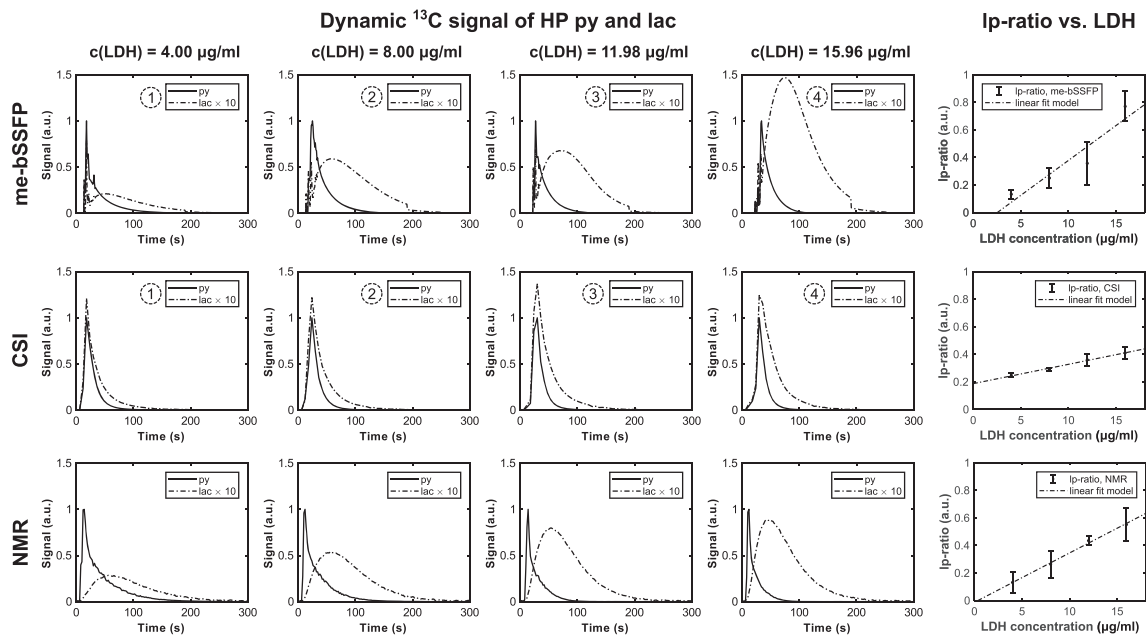
FIGURE 6 Time course of ^{13}C signal of HP pyruvate and lactate injected into different concentrations of LDH, acquired dynamically once a second with me-bSSFP (top), every 6 seconds with FID-CSI (middle) and every other second by NMR (bottom). The areas under the curves were calculated to yield the lactate-pyruvate (lp) ratios and a linear slope was fitted to the data (right). Increasing LDH concentrations (c (LDH)) resulted in increased lp ratio. Averages of either three me-bSSFP, three FID-CSI or four NMR scans are shown. Me-bSSFP was involuntarily acquired two times for 240 seconds and one time for 190 seconds

for me-bSSFP and FID-CSI, respectively (Figure 7B,C). The pyruvate signal in the whole animal, which is dominated by the signal from vascular pyruvate, decayed 10.0 ± 0.4 seconds faster for me-bSSFP compared with 13.9 ± 2.1 seconds for FID-CSI.

3.5 | 3D in vivo measurement of pyruvate to lactate conversion

Pyruvate was HP and injected 19 seconds after dissolution into a tumor-bearing animal inside the PET-MRI (duration of injection 26 seconds). Three consecutive 3D me-bSSFP acquisitions were started 45 seconds after dissolution (PET-MRI, protocol 5). Each 3D scan required 8.2 seconds. Sagittal images equidistant to the surface coil were reconstructed for pyruvate and lactate and coregistered on ^{1}H MRI (Figure 8, protocol 5). A 3D rotating view with maximum intensity projections of pyruvate and lactate coregistered on ^{1}H MRI is provided online (Movie S3).

Strong signals of pyruvate and lactate were found in the abdomen, blood vessels and liver, but also in the heart, kidneys and tumor. It should be emphasized that our measurement method was tailored to the observation of pyruvate, pyruvate hydrate and lactate relevant for our tumor study, so signals from other metabolites like [1–^{13}C]alanine and [^{13}C]bicarbonate (denoted as alanine and bicarbonate), which are expected to be present in some regions, were not detected.

Interestingly, the lactate signal within the tumor was very heterogeneous, possibly indicating variations in metabolic activity. Again, the lactate MS was accurately depicted, indicating an accurate metabolite separation. Reduced ^{1}H and ^{13}C signal was observed with increasing distance to the (surface) coil and at its edges; the coil did not encompass the entire animal. Substantially reduced SNR was observed in the images acquired 8.2 and 16.4 seconds after the onset of the first MRSI. Here, only some HP pyruvate signal was found in large blood vessels, but not in the tumor area, while constant signal was observed from the non-HP lactate MS next to the animal.

4 | DISCUSSION

4.1 | Analyzing the bSSFP signal response

As expected, it was crucial to choose the appropriate TR for mapping metabolites with me-bSSFP; it allows passing or suppressing the signal at different frequencies.[29,35,37] The results emphasize that the efficiency of bSSFP is strongly dependent on the choice of TRs and flip
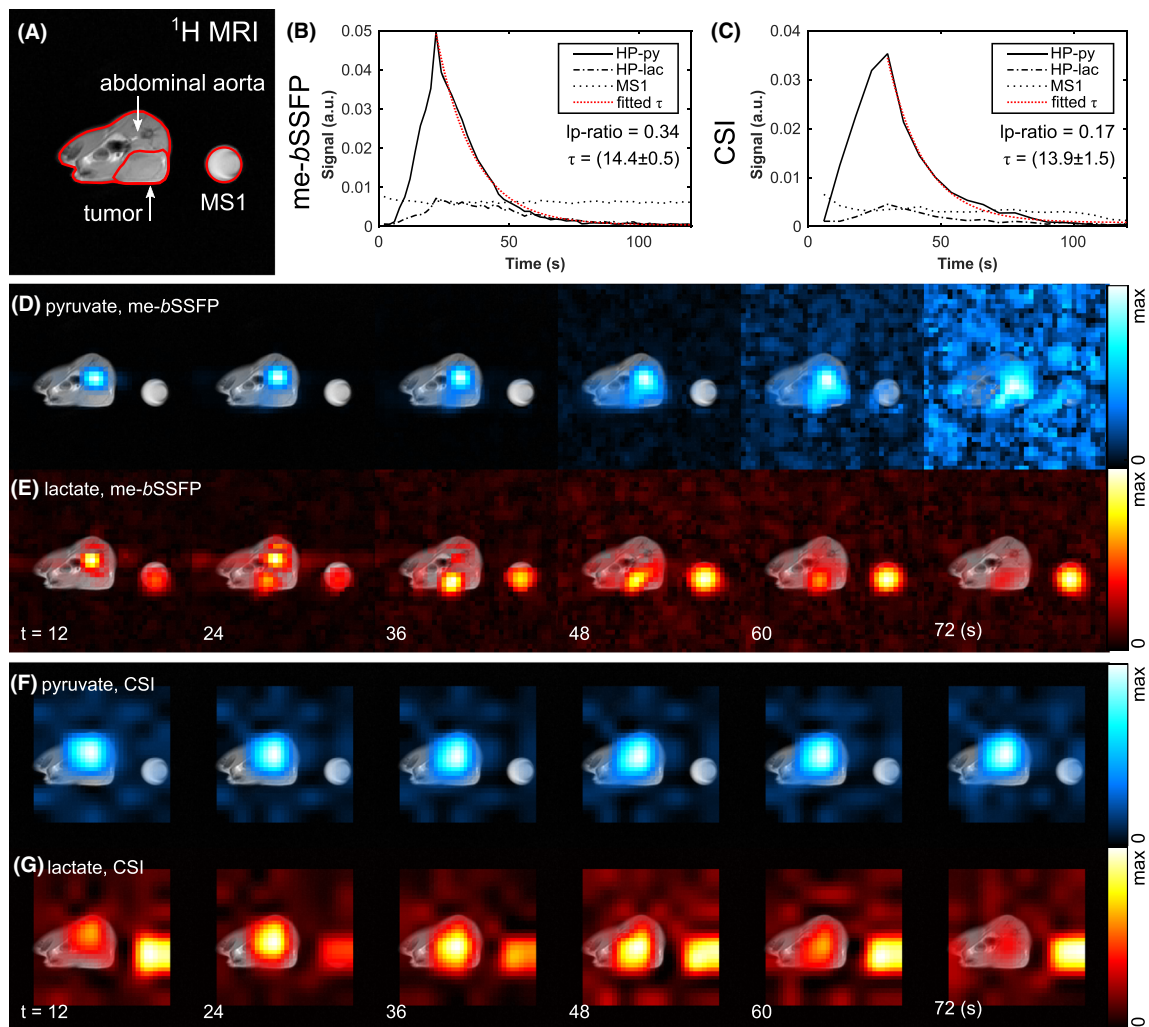
FIGURE 7 [1]H-MRI (A, gray), ^{13}C metabolite maps (E-G) and time course (B, C) of HP pyruvate (blue) and lactate (red) after injection of HP pyruvate into a tumor-bearing rat. The maps were acquired dynamically every 2 seconds with 2D me-bSSFP (D, E), every 6 seconds with 2D FID-CSI (F, G), and quantified in the regions indicated in A (B, C). Note the improved spatial resolution of me-bSSFP. Each metabolite image was individually scaled to its maximum. The diameter of MS1 was ~ 1.5 cm

angles; these parameters determine for how long the fate of the HP spins can be monitored. Simulated and experimental signal was found to coincide well, such that we used the simulations to identify optimal parameters for HP MRI, which cannot be repeated easily for parameter optimization.

The evolution of the signal within me-bSSFP scan time is a mix of T_1 decay for small flip angles and T_2 decay for large 180° as it was previously described analytically for on-resonant spins.[37] The off-resonances cause oscillatory response of the signal over different TRs, similar to reported previously.[29] With TRs being a multiple of the inverse off-resonance ω^{-1}, a quasi on-resonant condition is mimicked because the dephasing of spins between two pulses is a multiple of 2π. This results in signal evolution with the above weighting. Other TRs lead to dephasing of the off-resonant spins, resulting in a reduction of signal, which eventually is irreversible in MRI of HP agents.

In vitro, T_1 and T_2 can be measured and taken into account to choose the optimal flip angle; this was carried out and yielded good results (Figure 2). In vivo, T_1 of pyruvate and lactate was assumed to be in the range of 15 to 35 seconds.[38] It is not straightforward to measure T_2 in vivo. Effects such as flow, diffusion, conversion and relaxation overlap. It appears reasonable to assume the necessary relaxation properties and use the simulations to support an experimental optimization.

The situation is exacerbated further by the inhomogeneous excitation profile of surface coils. This issue was not treated by the simulations explicitly, but is likely mitigated by using volume coils instead. Note that the studies using thermally polarized phantoms were performed with a volume coil, while all HP experiments were conducted with surface coils due to availability of coils for the specific MRI. Using a surface coil leaves some uncertainties about the real flip angles that are applied by the inhomogeneous excitation profile of the coil (see S4 in Hundshammer et al,[39] in which the same coil was used). To minimize this issue, rather small flip angles were applied in the HP experiments, instead of the high flip angles that were suggested from simulations.
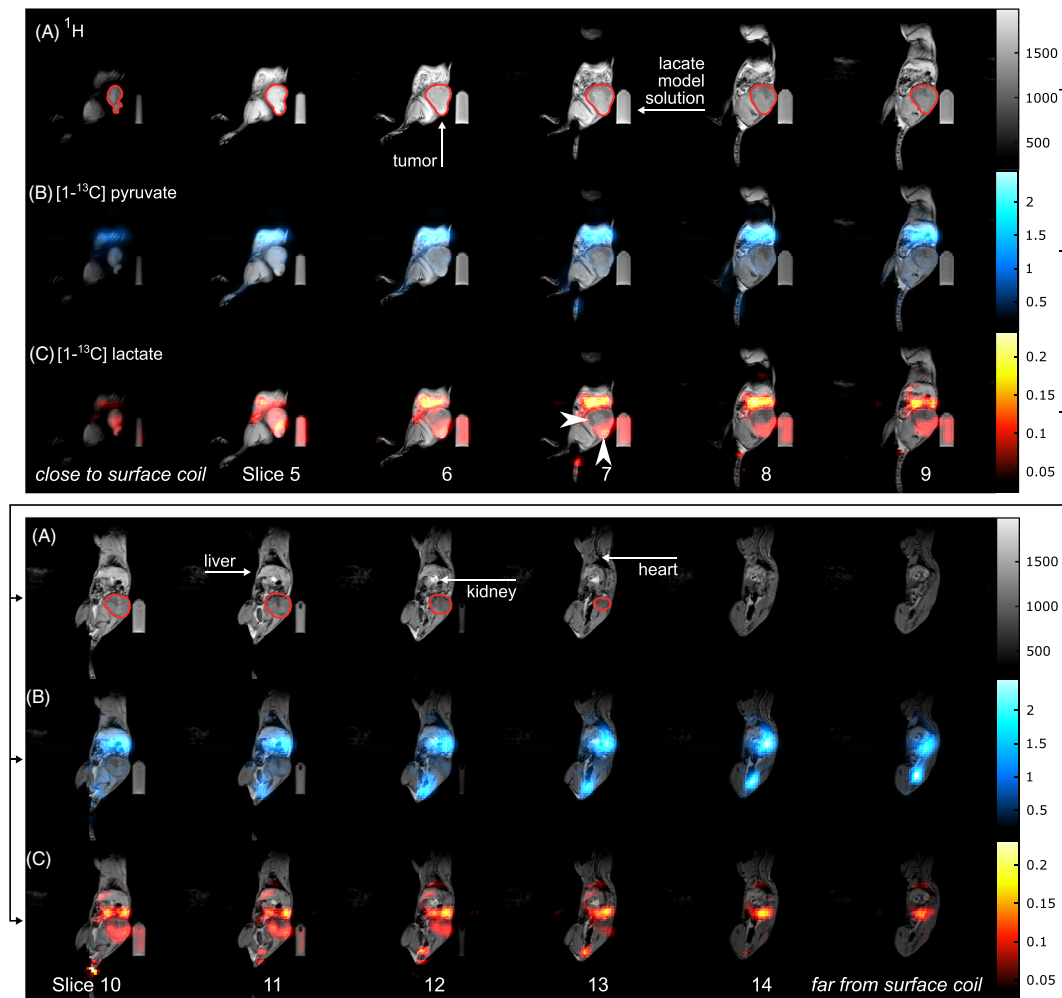
FIGURE 8 In vivo sagittal ^1H MRI (A, gray) and 3D ^{13}C metabolite maps of pyruvate (B, blue) and lactate (C, red) obtained with a 3D me-bSSFP after injection of HP pyruvate into a tumor-bearing rat in a scan time of 8.2 seconds (3 T PET-MR, protocol 4). The scan was started ~ 45 seconds after dissolution after the injection was finished. Strong signals of HP pyruvate and lactate were observed in the abdomen, the blood vessels, liver, kidneys and heart, in descending order of intensity. The subcutaneous tumor (A, red line) exhibited strong and spatially variable lactate signal (white arrows in slice 7). The slices shown are perpendicular to the coil axis and MS1 shows homogeneous lactate signal. Window and contrast of all images was adjusted to crop the noise signal outside the animal. Note the ^1H signal drop at a distance to the coil. Diameter and length of the lactate model solution are ~ 1.5 and 3.5 cm, respectively

It should also be noted that the absolute intensities of the metabolites are weighted by many factors, including relative frequency, TR, flip angle, T_1 and T_2.[37] Absolute quantification, for example, of the exchange kinetics, requires knowledge of all factors and appears to be difficult. Kinetic analysis with model-free approaches[36,40] only hold true if there is no particular weighting of one metabolite or the other. This effect occurs in one way or another for most sequences, and should be investigated throughout if a sequence is used for HP MRI by simulations.

4.2 | Decay of hyperpolarization during ^{13}C imaging

The lifetime of the HP spin state is a central criterion for the development of tracers. Likewise, sequences that use the magnetization efficiently are key.[41] Except for continuously HP tracers,[42,43] the total amount of polarization available is finite and can only be used once. At the same time, it is a goal to acquire several time points to investigate the metabolic dynamics.

Interestingly, me-bSSFP appears to be very efficient, consuming only very little polarization for each image. Part of the reason is that me-bSSFP is very fast: the magnetization is only for a very short time in the transversal state where the decay is faster (T_2 vs. T_1). In addition, remaining transversal magnetization is flipped back when it is no longer needed.

A commonly faced problem is that the signal of pyruvate is much stronger than that of lactate or other metabolites. This issue may be addressed by designing pulses that excite pyruvate less than the other metabolites, such that less pyruvate is used up and the signal intensities are similar.[44] The drawback of this approach are pulse widths of the order of 10 ms, which would dramatically increase the TR and scan time and reduce the efficiency of me-bSSFP. Placing pyruvate in one of the signal minima will reduce pyruvate signal but not preserve magnetization.

4.3 | In vitro and in vivo pyruvate and lactate imaging

Of course, an experimental comparison with more sophisticated methods than FID-CSI is important, but unfortunately, none of these methods were available to us in this study. Besides, FID-CSI is arguably still the most stable and widespread technique available. EPSI,[45,46] spiral CSI[47] and spiral IDEAL CSI[21] sequences have demonstrated similar spatial and temporal resolutions to me-bSSFP, with fewer excitations and shorter scan times than FID-CSI. Most recently, ^{13}C MRSI on clinical systems was reported in the literature with spatial resolutions of $5 \times 5 \times 23$ mm^3, FOV = $80 \times 80 \times 23$ mm^3 in 11 seconds[48,49]; $10 \times 10 \times 15$ mm^3, FOV = $160 \times 160 \times 15$ mm^3 in 4.3 seconds[11]; and $9.4 \times 5.6 \times 15$ mm^3, FOV = $150 \times 180 \times 15$ mm^3 in 1.3 seconds.[46] Here, with the developed 2D me-bSSFP, ^{13}C images were acquired with a spatial resolution of $5.6 \times 5.6 \times 10$ mm^3, FOV = $180 \times 180 \times 10$ mm^3 in 0.35 seconds. By not fully exploiting the temporal resolution and using a tip-back pulse to conserve the HP signals during times of no scanning, the sequence was efficient enough to dynamically image HP lactate in vitro and in vivo for at least up to 240 and 72 seconds, respectively. This is even more remarkable since a surface coil was used, and the overall HP magnetization appeared to be rather low.

No other metabolites were observed in the individual or summed spectrum of all CSI voxels (Figure S4). That neither alanine nor bicarbonate was measurable might be attributed to low concentrations and low sensitivity of the surface coil in the regions where these metabolites are produced. However, the limited number of me-bSSFP echoes acquired did not allow for the reconstruction of more metabolites besides pyruvate, pyruvate hydrate and lactate. How well me-bSSFP will perform for imaging more metabolites will have to be investigated. With implementation of more echoes into me-bSSFP and using a different TR, alanine or bicarbonate images could also be reconstructed. However, care must be taken with respect to the frequency response of bSSFP. Using the intrinsic off-resonance sensitivity of bSSFP can also yield metabolic information in very short scan times by using progressive pulse phase and flip angle schemes.[50] For this method, a B_0 field map acquisition was required. With me-bSSFP and the used IDEAL decomposition, a B_0 field estimation based on the ^{13}C signal comes at no cost (Figure S5).

4.4 | 3D in vivo measurement of pyruvate to lactate conversion

Selective imaging of either HP pyruvate or lactate with frequency-selective bSSFP has been reported: pyruvate or lactate images were acquired in 1.8 seconds, each containing a resolution of $2.5 \times 2.5 \times 2.5$ mm^3 in a $80 \times 40 \times 40$ mm^3 FOV (220 μs/voxel) of tumor-bearing animals at 3 T using animal volume coils.[33] Alanine and pyruvate hydrate signals were suppressed prior to each acquisition.

Here, we demonstrated dynamic 3D ^{13}C MRSI of pyruvate and lactate with a spatial resolution of $5.6 \times 5.6 \times 2$ mm^3 in a $180 \times 180 \times 48$ mm^3 FOV in a scan time of 8.2 seconds (333 μs/voxel). Taking into account that the frequency-selective bSSFP above requires two scans each of 1.8 seconds for a set of one pyruvate and one lactate map, plus the different FOV and spatial resolutions of the two methods, the temporal resolution, as in scan time per voxel, was very similar.[33] It should be emphasized that time per voxel gives only an approximate figure for the dynamic performance of an acquisition method, since the number of voxels can be easily tweaked by, for example, over- or undersampling.

In the in vivo 3D me-bSSFP scans, different lactate intensities inside the tumor indicate metabolic heterogeneity. This result is plausible, because 2D MRSI is likely to underestimate tumor heterogeneity if a thick slice is used (eg, 10 mm or more). Here, much thinner slices were used (2 mm).

The reduction of HP signal in the second and third consecutive 3D scans can be attributed to the long scan time of me-bSSFP and the long train of RF pulses that were needed for full 3D encoding. Note that the 3D me-bSSFP scans were also conducted with a higher flip angle than the 2D scans. The uncertainty of flip angles played out by surface coils was already discussed above. Additionally, as some of the moving HP spins will have temporarily left the excitation volume during imaging, parts of the agent will not have been exposed to the full me-bSSFP sequence. This drastically reduces the efficiency of the refocusing strategy of me-bSSFP.

4.5 | Measuring the LP ratio

The LP ratio was previously shown to be proportional to the conversion rate constant from pyruvate to lactate k_{PL}, and inversely proportional to the sum of the reverse flux from lactate to pyruvate k_{LP} and the effective relaxation rate of HP lactate r_L.[36]

In the in vitro measurements with different LDH concentrations it was valid to neglect the reverse flux k_{LP}, since HP pyruvate has the dominant concentration in the solution. The effective relaxation of HP lactate r_L is dependent on the intrinsic relaxation and the signal loss due to RF excitations through the used sequence. While the LP ratios measured in vitro with me-bSSFP and NMR were in good agreement, differences were apparent to those obtained by FID-CSI.

The metabolite maps obtained from FID-CSI in vitro and in vivo exhibited both low SNR and artifacts across the FOV. This observation was made in all CSI in vitro experiments. The artifacts in vitro may be explained by the rectangular arrangement of the vials in parallel to the gradient encoding and the broad point spread function (PSF) of the elliptically sampled k-space, which led to a superposition of multiple signals within each individual vial and thus affected the measurement of the LP ratio. Also, in vivo, the PSF of the elliptically sampled k-space of FID-CSI resulted in rather strong signal peaks of the HP pyruvate being measured, even outside the animal. This induces a bias in the variability of the noise and thus on the measurement of SNR in the FID-CSI maps and was the reason why signal intensity and not SNR was used for calculation of the LP ratio.

The difference in LP ratio in vivo (factor two) between me-bSSFP and FID-CSI may additionally originate from the poor spatial separation of blood and tumor signals on the FID-CSI images: [13]C signal from the vessels is found in the tumor region and vice versa, resulting in an overestimation of the tumor ^{13}C signal. If the pyruvate blood concentration is high, this effect is stronger for pyruvate than for lactate, resulting in a reduced LP ratio inside the tumor. A parallel study verified that the LP ratio correlates with the distance between tumor and abdominal artery and with the size of the tumor when measured with FID-CSI.[39] Due to the increased spatial resolution, the separation between abdominal artery and tumor tissue was clearer in the me-bSSFP maps than in the FID-CSI maps. Both methods detected lactate in the animal's abdominal artery. This observation results from either incorrect reconstruction of the metabolite maps at very high pyruvate intensities or from actual lactate in the blood pool, as was previously reported.[51]

The accuracy of the IDEAL reconstruction is difficult to assess. The strongly undersampled spectral information and the reconstruction at selected frequencies might project signal into the metabolite maps that arises from neglected, albeit much smaller, resonances, that is, alanine or bicarbonate. Most likely this is not an issue for the current study because no other resonances were observed in the CSI data in vivo even if all spectra were summed (see Figure S4). Other critical points are the strong differences in signal intensities and the evolution of pyruvate and lactate signal during k-space acquisition, which may not be the same. This effect is small for 2D imaging because of the short acquisition times (<1 second), but is more pronounced in 3D MRI, where the acquisition times exceed several seconds. The research here is ongoing and there is potential to improve the IDEAL reconstruction, that is, with the input of an acquired B_0 map and by computing the decomposition in k-space instead of in image domain.[52]

Further measures to assure the quality of the metabolite separation and quantification are needed. Already, some confidence was provided by a lactate MS that was placed next to the animal. The lactate signal of the solution was reconstructed well in all MRSI experiments, with no apparent contribution to the pyruvate images, and the intensity was constant during dynamic acquisitions. We envision a multi-compartment phantom containing MSs of all metabolites, namely, pyruvate, lactate, alanine and bicarbonate, placed next to the subject during HP-MRSI.

5 | CONCLUSIONS

The results obtained from dynamic me-bSSFP[28,29] and IDEAL[26] reconstruction provided fast and very efficient imaging of HP pyruvate and lactate. In contrast to conventional spectroscopic imaging, the method provides a limited chemical shift resolution, which can be adapted to the question at hand, and a high spatial and temporal resolution while consuming only little HP magnetization.

Simulating the signal evolution helped to identify favorable sequence parameters and to avoid known bSSFP artefacts. A careful selection of sequence parameters was essential to obtain a smooth signal evolution throughout the sequence.

With the developed 2D me-bSSFP protocol, the enzymatic conversion of HP pyruvate to lactate was observed for up to 240 seconds in vitro and 72 seconds in vivo. In addition, 3D metabolite mapping with me-bSSFP was successfully demonstrated with a short scan time. 3D imaging may enable new insights in heterogeneous structural differences inside tumor tissue. Dynamic 3D scanning may be enabled by reducing the number and flip angle of the RF pulses.

Using more homogeneous volume coils seems highly preferable for HP ^{13}C MRSI, that is, using volumetric coils for excitation to reach the optimal flip angles, and using surface coils with higher sensitivity for receiving the HP magnetization.

The outcomes of kinetic activity measurements with HP ^{13}C MRSI (ie, LP ratio) depend strongly on the acquisition strategy. The standardization of measurement methods and postprocessing will be important for translation into clinical routine.

In the absence of actual spectra, an MS containing all metabolites of interest in different compartments would improve confidence in assuring the quality of the metabolite separation.

In any case of interest in acquiring the simulation or reconstruction code, please contact the corresponding author in the first instance.

ORCID

Christoph A. Müller https://orcid.org/0000-0002-8187-9170
Christian Hundshammer https://orcid.org/0000-0002-6738-1560

REFERENCES

1. Xu V, Chan H, Lin AP, et al. MR spectroscopy in diagnosis and neurological decision-making. *Semin Neurol*. 2008;28(4):407-422.
2. Ardenkjær-Larsen JH, Fridlund B, Gram A, et al. Increase in signal-to-noise ratio of > 10,000 times in liquid-state NMR. *PNAS*. 2003;100(18):10158-10163.
3. Achtnichts L, Amann M, Hirsch J, et al. Assessment of whole brain N-acetylaspartate – a new additional MR marker in mild cognitive impairment and Alzheimer's disease. *Akt Neurol*. 2007;34(S2):V231.
4. Barker PB, Hearshen DO, Boska MD. Single-voxel proton MRS of the human brain at 1.5T and 3.0T. *Magn Reson Med*. 2001;45(5):765-769.
5. Brown TR, Kincaid BM, Ugurbil K. NMR chemical shift imaging in three dimensions. *PNAS*. 1982;79(11):3523-3526.
6. Maudsley AA, Hilal SK, Perman WH, Simon HE. Spatially resolved high resolution spectroscopy by "four-dimensional" NMR. *J Magn Reson*. 1983;51(1):147-152.
7. Mayer D, Yen Y-F, Levin YS, et al. In vivo application of sub-second spiral chemical shift imaging (CSI) to hyperpolarized 13C metabolic imaging: Comparison with phase-encoded CSI. *J Magn Reson*. 2010;204(2):340-345.
8. Posse S, Tedeschi G, Risinger R, Ogg R, Bihan DL. High speed 1H spectroscopic imaging in human brain by echo planar spatial-spectral encoding. *Magn Reson Med*. 1995;33(1):34-40.
9. Mulkern RV, Panych LP. Echo planar spectroscopic imaging. *Concepts Magn Reson*. 2001;13(4):213-237.
10. Park I, Larson PEZ, Gordon JW, et al. Development of methods and feasibility of using hyperpolarized carbon-13 imaging data for evaluating brain metabolism in patient studies. *Magn Reson Med*. 2018;80(3):864-873.
11. Miloushev VZ, Granlund KL, Boltyanskiy R, et al. Metabolic imaging of the human brain with hyperpolarized 13C pyruvate demonstrates 13C lactate production in brain tumor patients. *Cancer Res*. 2018;78:3755-3760.
12. Lee H, Song JE, Shin J, et al. High resolution hyperpolarized 13C MRSI using SPICE at 9.4T. *Magn Reson Med*. 2018;80(2):703-710.
13. Lau JYC, Geraghty BJ, Chen AP, Cunningham CH. Improved tolerance to off-resonance in spectral-spatial EPI of hyperpolarized [1-¹³C]pyruvate and metabolites: improved tolerance to off-resonance in ¹³C EPI. *Magn Reson Med*. 2018;80(3):925-934.
14. Dixon WT. Simple proton spectroscopic imaging. *Radiology*. 1984;153(1):189-194.
15. Yeung HN, Kormos DW. Separation of true fat and water images by correcting magnetic field inhomogeneity in situ. *Radiology*. 1986;159(3):783-786.
16. Glover GH, Schneider E. Three-point dixon technique for true water/fat decomposition with B0 inhomogeneity correction. *Magn Reson Med*. 1991;18(2):371-383.
17. Glover GH. Multipoint Dixon technique for water and fat proton and susceptibility imaging. *J Magn Reson Imaging*. 1991;1(5):521-530.
18. Reeder SB, Wen Z, Yu H, et al. Multicoil Dixon chemical species separation with an iterative least-squares estimation method. *Magn Reson Med*. 2004;51(1):35-45.
19. Reeder SB, Pineda AR, Wen Z, et al. Iterative decomposition of water and fat with echo asymmetry and least-squares estimation (IDEAL): Application with fast spin-echo imaging. *Magn Reson Med*. 2005;54(3):636-644.
20. Wiens CN, Friesen-Waldner LJ, Wade TP, Sinclair KJ, McKenzie CA. Chemical shift encoded imaging of hyperpolarized 13C pyruvate. *Magn Reson Med*. 2015;74(6):1682-1689.
21. Wiesinger F, Weidl E, Menzel MI, et al. IDEAL spiral CSI for dynamic metabolic MR imaging of hyperpolarized [1-13C]pyruvate. *Magn Reson Med*. 2012;68(1):8-16.
22. Friesen-Waldner LJ, Sinclair KJ, Wade TP, et al. Hyperpolarized [1-13C]pyruvate MRI for noninvasive examination of placental metabolism and nutrient transport: A feasibility study in pregnant guinea pigs. *J Magn Reson Imaging*. 2016;43(3):750-755.
23. Gordon JW, Niles DJ, Fain SB, Johnson KM. Joint spatial-spectral reconstruction and k-t spirals for accelerated 2D spatial/1D spectral imaging of 13C dynamics. *Magn Reson Med*. 2014;71(4):1435-1445.
24. Yu H, McKenzie CA, Shimakawa A, et al. Multiecho reconstruction for simultaneous water-fat decomposition and T2* estimation. *J Magn Reson Imaging*. 2007;26(4):1153-1161.
25. Yu H, Shimakawa A, McKenzie CA, Brodsky E, Brittain JH, Reeder SB. Multiecho water-fat separation and simultaneous R estimation with multi-frequency fat spectrum modeling. *Magn Reson Med*. 2008;60(5):1122-1134.
26. Peterson P, Månsson S. Fat quantification using multiecho sequences with bipolar gradients: Investigation of accuracy and noise performance. *Magn Reson Med*. 2014;71(1):219-229.
27. Scheffler K. Fast frequency mapping with balanced SSFP: Theory and application to proton-resonance frequency shift thermometry. *Magn Reson Med*. 2004;51(6):1205-1211.
28. Leupold J, Wieben O, Månsson S, et al. Fast chemical shift mapping with multiecho balanced SSFP. *Magn Reson Mater Phy*. 2006;19(5):267-273.
29. Leupold J, Månsson S, Petersson JS, Hennig J, Wieben O. Fast multiecho balanced SSFP metabolite mapping of 1H and hyperpolarized 13C compounds. *Magn Reson Mater Phy*. 2009;22(4):251-256.

30. Perman WH, Bhattacharya P, Leupold J, et al. Fast volumetric spatial-spectral MR imaging of hyperpolarized 13C-labeled compounds using multiple echo 3D bSSFP. *Magn Reson Imaging*. 2010;28(4):459-465.

31. von Morze C, Sukumar S, Reed GD, et al. Frequency-specific SSFP for hyperpolarized 13C metabolic imaging at 14.1 T. *Magn Reson Imaging*. 2013;31(2):163-170.

32. Milshteyn E, von Morze C, Reed GD, et al. Development of high resolution 3D hyperpolarized carbon-13 MR molecular imaging techniques. *Magn Reson Imaging*. 2017;38(Suppl C):152-162.

33. Milshteyn E, von Morze C, Gordon JW, Zhu Z, Larson PEZ, Vigneron DB. High spatiotemporal resolution bSSFP imaging of hyperpolarized [1-13C] pyruvate and [1-13C]lactate with spectral suppression of alanine and pyruvate-hydrate. *Magn Reson Med*. 2018;80(3):1048-1060.

34. Oppelt A, Graumann R, Barfuss H, Fischer H, Hartl W, Schajor W. FISP, a novel, fast pulse sequence for nuclear magnetic resonance imaging. *Electromedica*. 1986;54(1):15-18.

35. Scheffler K, Lehnhardt S. Principles and applications of balanced SSFP techniques. *Eur Radiol*. 2003;13(11):2409-2418.

36. Liang Z-P, Lauterbur PC. Principles of Magnetic Resonance Imaging: A Signal Processing Perspective. New York, NY: Wiley; 1999.

37. Hill DK, Orton MR, Mariotti E, et al. Model free approach to kinetic analysis of real-time hyperpolarized 13C magnetic resonance spectroscopy data. *PLOS One*. 2013;8(9):e71996.

38. Scheffler K. On the transient phase of balanced SSFP sequences. *Magn Reson Med*. 2003;49(4):781-783.

39. Larson PEZ, Chen H-Y, Gordon JW, et al. Investigation of analysis methods for hyperpolarized 13C-pyruvate metabolic MRI in prostate cancer patients. *NMR Biomed*. 2018;31(11):e3997.

40. Hundshammer C, Braeuer M, Müller CA, et al. Simultaneous characterization of tumor cellularity and the Warburg effect with PET, MRI and hyperpolarized 13C-MRSI. *Theranostics*. 2018;8(17):4765-4780.

41. Daniels CJ, McLean MA, Schulte RF, et al. A comparison of quantitative methods for clinical imaging with hyperpolarized 13C-pyruvate. *NMR Biomed*. 2016;29(4):387-399.

42. Brindle KM. Imaging metabolism with hyperpolarized 13C-labeled cell substrates. *J Am Chem Soc*. 2015;137(20):6418-6427.

43. Rovedo P, Knecht S, Bäumlisberger T, et al. Molecular MRI in the Earth's magnetic field using continuous hyperpolarization of a biomolecule in water. *J Phys Chem B*. 2016;120(25):5670-5677.

44. Hövener J-B, Schwaderlapp N, Lickert T, et al. A hyperpolarized equilibrium for magnetic resonance. *Nat Commun*. 2013;4:2946.

45. Larson PEZ, Kerr AB, Chen AP, et al. Multiband excitation pulses for hyperpolarized 13C dynamic chemical-shift imaging. *J Magn Reson*. 2008;194(1):121-127.

46. Yen Y-F, Kohler SJ, Chen AP, et al. Imaging considerations for in vivo 13C metabolic mapping using hyperpolarized 13C-pyruvate. *Magn Reson Med*. 2009;62(1):1-10.

47. Eldirdiri A, Posse S, Hanson LG, et al. Development of a symmetric echo-planar spectroscopy imaging framework for hyperpolarized 13C imaging in a clinical PET/MR scanner. *Tomography*. 2018;4(3):110-122.

48. Mayer D, Levin YS, Hurd RE, Glover GH, Spielman DM. Fast metabolic imaging of systems with sparse spectra: Application for hyperpolarized13C imaging. *Magn Reson Med*. 2006;56(4):932-937.

49. Gutte H, Hansen AE, Henriksen ST, et al. Simultaneous hyperpolarized 13C-pyruvate MRI and 18F-FDG-PET in cancer (hyperPET): feasibility of a new imaging concept using a clinical PET/MRI scanner. *Am J Nucl Med Mol Imaging*. 2014;5(1):38-45.

50. Gutte H, Hansen AE, Larsen MME, et al. Simultaneous hyperpolarized 13C-pyruvate MRI and 18F-FDG PET (hyperPET) in 10 dogs with cancer. *J Nucl Med*. 2015;56(11):1786-1792.

51. Varma G, Wang X, Vinogradov E, et al. Selective spectroscopic imaging of hyperpolarized pyruvate and its metabolites using a single-echo variable phase advance method in balanced SSFP. *Magn Reson Med*. 2016;76(4):1102-1115.

52. Wespi P, Steinhauser J, Kwiatkowski G, Kozerke S. Overestimation of cardiac lactate production caused by liver metabolism of hyperpolarized [1–13C]pyruvate. *Magn Reson Med*. 2018;80(5):1882-1890.

53. Brodsky EK, Holmes JH, Yu H, Reeder SB. Generalized k-space decomposition with chemical shift correction for non-cartesian water-fat imaging. *Magn Reson Med*. 2008;59(5):1151-1164.

SUPPORTING INFORMATION

Additional supporting information may be found online in the Supporting Information section at the end of this article.